nature neuroscience

Large-scale cortical correlation structure of spontaneous oscillatory activity

Joerg F Hipp[1,2], David J Hawellek[1], Maurizio Corbetta[3], Markus Siegel[2] & Andreas K Engel[1]

Little is known about the brain-wide correlation of electrophysiological signals. We found that spontaneous oscillatory neuronal activity exhibited frequency-specific spatial correlation structure in the human brain. We developed an analysis approach that discounts spurious correlation of signal power caused by the limited spatial resolution of electrophysiological measures. We applied this approach to source estimates of spontaneous neuronal activity reconstructed from magnetoencephalography. Overall, correlation of power across cortical regions was strongest in the alpha to beta frequency range (8–32 Hz) and correlation patterns depended on the underlying oscillation frequency. Global hubs resided in the medial temporal lobe in the theta frequency range (4–6 Hz), in lateral parietal areas in the alpha to beta frequency range (8–23 Hz) and in sensorimotor areas for higher frequencies (32–45 Hz). Our data suggest that interactions in various large-scale cortical networks may be reflected in frequency-specific power envelope correlations.

As a measure of functional connectivity, the co-variation of spontaneous hemodynamic signals has revealed fundamental insights into the large-scale functional organization of the human brain[1,2]. Blood oxygen level–dependent functional magnetic resonance imaging (BOLD fMRI) has provided consistent evidence for correlated fluctuations of spontaneous neuronal activity in highly structured networks of brain regions[3–9]. The gross spatial correlation structure that constitutes these networks is highly robust and often studied during resting fixation. Furthermore, the correlation structure also reflects task demands[8,10], the subjects' conscious state[11], and psychiatric and neurological disorders[12,13].

However, an important limitation of the available fMRI studies is that hemodynamic signals only provide an indirect measure of neuronal activity[14–16]. In contrast, electroencephalography (EEG) and magnetoencephalography (MEG) directly measure the electrophysiological activity of interest. Furthermore, with their high temporal resolution, these electrophysiological measures sample the rich temporal dynamics of neuronal population activity. These temporal dynamics entail neuronal oscillations that, with their specific frequencies, reflect the biophysical properties of different local and large-scale network interactions[17–19]. Thus, connectivity measures based on specific spectral components of neuronal population activity may provide qualitatively new insights into the circuit mechanisms underlying the large-scale organization of brain activity[19]. However, little is known about the brain-wide correlation of such frequency-specific neuronal population signals. To characterize the brain-wide correlation structure of oscillatory power, we developed a new analysis approach for investigating large-scale functional connectivity that overcomes current methodological limitations in EEG and MEG. We applied this approach to MEG recordings of healthy human subjects during resting fixation.

RESULTS

We recorded MEG from 43 subjects that were instructed to fixate a centrally presented cross (average duration, ~500 s). We applied time-frequency transformation and linear 'beamforming' to the MEG data to derive temporally, spectrally and spatially resolved estimates of neuronal population activity. The temporal evolution of spectral power (power envelope) in different brain regions around a given carrier frequency served as the signal for our correlation analysis[20] (**Fig. 1a**). Notably, the correlation between power envelopes that we investigated should not be confused with measures of the phase relation between the underlying signals, such as coherence[19,21–23].

It is difficult to investigate the relationship between neuronal population signals from EEG and MEG because of notable methodological problems[19,23–25]. As a result of the limited spatial resolution of EEG and MEG, even distant sensors or source estimates can be sensitive to the same neuronal sources. In source space, this translates into a trivial spatial interaction pattern that drops off with distance from any reference location. **Figure 1b** illustrates this problem for the power envelope correlation between a reference location in the left somatosensory cortex and the rest of the brain. The spatial correlation pattern is dominated by an unstructured decay from the reference site that is caused by the fact that source estimates close to the reference location are sensitive to the same true sources as the reference estimate. This spurious correlation pattern is problematic, as it masks the physiological correlation structures of interest. To overcome this problem, we developed a new analysis approach for studying functional connectivity based on power envelope correlations.

Power envelope correlation between orthogonalized signals

Electrical and magnetic neuronal signals are measured virtually instantaneously at different sensors. Thus, signal components that reflect the

[1]Department of Neurophysiology and Pathophysiology, University Medical Center Hamburg-Eppendorf, Hamburg, Germany. [2]Centre for Integrative Neuroscience, University of Tübingen, Tübingen, Germany. [3]Departments of Neurology, Radiology, Anatomy, and Neurobiology, Washington University School of Medicine, St. Louis, Missouri. Correspondence should be addressed to J.F.H. (joerg.hipp@cin.uni-tuebingen.de).

Received 13 February; accepted 4 April; published online 6 May 2012; doi:10.1038/nn.3101

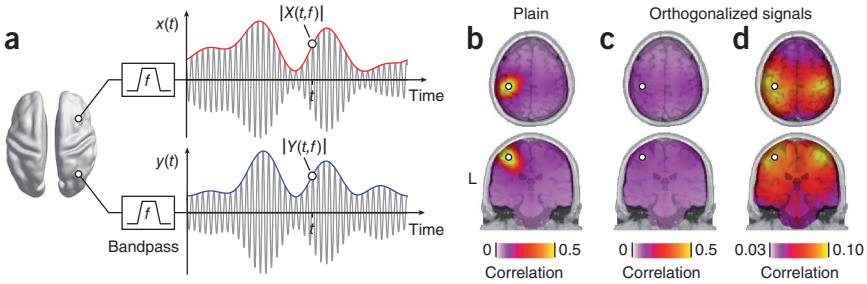

Figure 1 Power envelope correlation. (**a**) Illustration of spectrally resolved power envelopes for one exemplary carrier frequency *f* (that is, center frequency of the bandpass filter). The gray sinusoidal lines represent bandpass-filtered neuronal signals estimated at two source locations. The corresponding blue and red lines, the amplitude envelopes, quantify the evolution of the signal amplitude at a slower timescale. We used the logarithm of the squared amplitude envelopes (power envelopes) for correlation analyses. (**b**) Plain power envelope correlation between the left somatosensory cortex (white circle) and the rest of the brain at a carrier frequency of 16 Hz. The correlation values are overlaid on cortical slices intersecting the seed location. L, left. (**c**) Power envelope correlation between orthogonalized signals from the left somatosensory cortex (white circle) and the rest of the brain at a carrier frequency of 16 Hz. Note that the color scale is identical to that used in **b**. (**d**) Data are presented as in **c**, but scaled to the minimal and maximal correlation value that occurs.

same source at two different sensors (or source estimates) are characterized by an identical phase[24]. In contrast, for many cases, signals from different neuronal populations can be thought of as having a variable phase relation. We exploited this difference to discount the spurious correlation pattern caused by the limited spatial resolution of MEG. For each pair of signals, time window and carrier frequency, we removed the signal components that shared the same phase before computing the signals' power estimates. In other words, we orthogonalized the signals before deriving their power envelopes. As a measure of interaction, we then computed the linear correlation between these power envelopes. This procedure ensures that the signals do not share the trivial correlation in power resulting from the methodological problems described above (see Online Methods, **Supplementary Data** and **Supplementary Figs. 1** and **2**). Applying this approach to the above example had a strong effect. The pattern that dominated the plain correlation vanished, which revealed residual correlation of much smaller magnitude (**Fig. 1c**). This residual spatial correlation pattern was highly structured and extended to distant cortical areas (**Fig. 1d**). Correlation was strongest to the vicinity of the reference and to the homologous somatosensory cortex in the other hemisphere.

We next derived the correlation between all 2,925 locations on a regular three-dimensional grid covering the entire brain. The average correlation was significantly higher than zero for all carrier frequencies from 2 to 128 Hz (*t* test, $P < 0.05$, false discovery rate (FDR) corrected). The average correlation was strongest in the alpha to beta frequency range ($r = 0.069 \pm 0.060$, mean ± s.d. at 16 Hz) with about 90% of positive correlations. To identify spatial structure in the correlation, we statistically tested for correlation higher than the average correlation across the brain. As a starting point, we followed up on the introductory example and analyzed interhemispheric correlation between homologous early sensory areas across different modalities.

Interhemispheric correlation of homologous sensory areas

A fundamental property of human brain anatomy is that most homologous areas in the two hemispheres are anatomically connected. Accordingly, fMRI studies[1,26], intracranial recordings[27] and MEG studies[28,29] have found that homologous sensory areas exhibit correlated spontaneous activity. Consequently, we expected to find a related pattern for power envelope correlations using our new analysis approach.

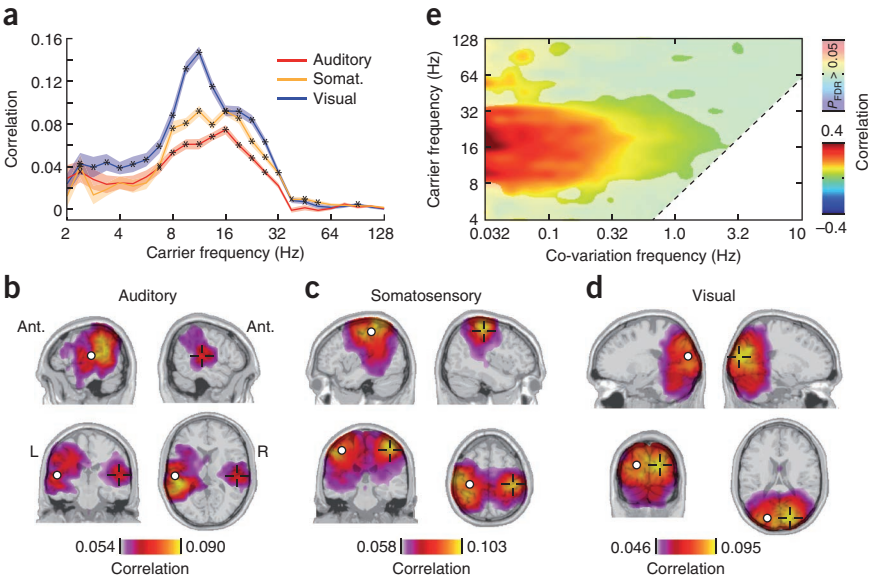

Figure 2 Power envelope correlations between orthogonalized spontaneous signals from homologous early sensory areas. (**a**) Correlation between the auditory cortices (red), the somatosensory cortices (Somat.) (yellow) and the visual cortices (blue) resolved for carrier frequency. Colored bands indicate the s.e.m. across subjects. Spatial specificity is tested by comparison to the average correlation with the rest of the brain (one-tailed *t* test, $^{x}P < 0.05$, $^{*}P < 0.01$; see **Supplementary Fig. 3a**,**b** for a control analyses with different spectral smoothing). (**b**–**d**) Spatial distribution of the correlation between the left auditory (**b**), somatosensory (**c**) and visual (**d**) cortices and the rest of the brain. Correlation values are statistically masked (one-tailed *t* test for correlation > average correlation with the rest of the brain, $P < 0.05$, FDR corrected for number of voxel). White circles indicate the location of the reference site and the crosses indicate the mirrored location in the other hemisphere. Ant., anterior; L, left; R, right. (**e**) Correlation between homologous sensory areas as a function of the carrier frequency and the co-variation frequency (center frequency of the bandpass applied to the power envelopes before computing correlation on the second level). Note that the highest co-variation frequency is limited by the underlying carrier frequency (diagonal dashed line). The values are averaged across sensory modalities and subjects and are statistically masked (one-tailed *t* test for correlation > average correlation to the rest of the brain, $P < 0.05$, FDR corrected for the number of carrier and co-variation frequencies; see **Supplementary Fig. 3c,d** for control analyses with different spectral parameters).

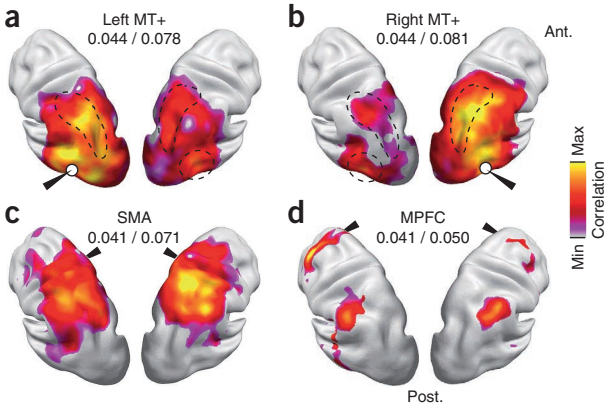

Figure 3 Correlation maps for selected locations at a carrier frequency of 16 Hz. Correlation maps are statistically masked (voxel-wise one-sided *t* test for correlation > average correlation to the rest of the brain, $P < 0.05$, FDR corrected for the number of voxels). The white circles indicate the approximate location of the seeds. The values underneath the seed labels indicate the minimal (min) and maximal (max) correlation in the statistical mask. (**a**,**b**) Left and right MT+. The homologous area in the other hemisphere and the intraparietal sulci are depicted by dashed lines. (**c**) SMA. (**d**) MPFC. Post., posterior.

We focused on bilateral early auditory, visual and somatosensory cortices and investigated a broad range of different carrier frequencies (**Fig. 2a**). In all three sensory systems, we found the strongest correlation in the alpha to beta carrier frequency range (8–32 Hz). The analysis of the brain-wide correlation at 16 Hz, the center of this frequency range, revealed that the correlation between homologous sensory cortices was spatially specific (one-sided *t* test for correlation > average correlation, $P < 0.05$, FDR corrected; **Fig. 2b–d**). The strongest correlations were expressed to areas in direct proximity of the reference locations and to the homologous cortex in the contralateral hemisphere.

We spectrally resolved the power envelope correlation (co-variation frequency; **Fig. 2e**) to assess its temporal scale. The correlation between homologous areas was significantly increased in a broad, low co-variation frequency range from 0.032 Hz (the lowest frequency analyzed) to above 1 Hz (one-sided *t* test for correlation > average correlation, $P < 0.05$, FDR corrected). Thus, modulation of signal power on the timescale of several seconds drove the correlation of spontaneous activity between sensory areas. These findings were insensitive to specific parameters of spectral analyses. We varied the spectral smoothing of the carrier and the co-variation frequencies and obtained similar results (**Supplementary Fig. 3**). In summary, our analysis approach revealed that spontaneous oscillatory population activity in different homologous early sensory cortices was correlated on a slow timescale in a spatially and spectrally specific manner.

Spatially specific correlation of higher order cortices

We next extended our analysis beyond early sensory regions and investigated how functional relations of higher order cortices are reflected in power correlations. We characterized correlation maps of a higher visual area, a higher sensory-motor area and a prefrontal associative area for a 16-Hz carrier frequency. The middle temporal area (MT+) is part of the dorsal visual pathway. Indeed, correlation with left and right MT+ peaked in the homologous area in the contralateral hemisphere and in the dorsal visual pathway along the intraparietal sulcus (one-sided *t* test for correlation > average correlation, $P < 0.05$, FDR corrected; **Fig. 3a**,**b**). Correlation with the supplementary motor area (SMA), which is part of the sensory-motor cortex involved in planning of movements, peaked in frontal regions that are compatible with the frontal eye fields and other regions in the parietal cortex (one-sided *t* test for correlation > average correlation, $P < 0.05$, FDR corrected; **Fig. 3c**). Also the medial prefrontal cortex (MPFC), a higher order associative area, exhibited spatially well-confined and symmetric correlation patterns (one-sided *t* test for correlation > average correlation, $P < 0.05$, FDR corrected; **Fig. 3d**). Correlation with MPFC peaked in bilateral dorsal prefrontal cortex (DPFC) and bilateral lateral parietal cortex (LPC).

The differences between the correlation patterns of these reference sites indicate that power envelope correlations can reveal distinct functional networks. However, the different correlation patterns also shared similar features. In particular, most reference sites showed a high correlation with parietal areas. This raised the question of whether specific areas such as the parietal cortex might have a particularly prominent role in the global patterning of power envelope correlations. We studied the correlation of power envelopes across the full cortico-cortical space to address this question.

Global correlation structure

We derived the full connectivity matrix between 2,925 sources (nodes) that covered the brain in a regular three-dimensional grid. We defined

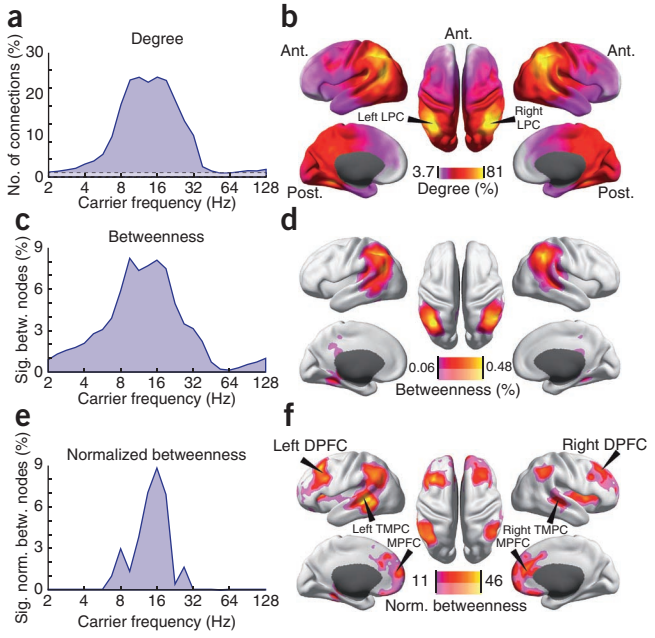

Figure 4 Graph-theoretical analysis of the global correlation structure of band-limited neuronal signals. (**a**) Spectrally resolved degree. The dashed line indicates the significance threshold (1.01%, $P = 0.05$, corrected for the number of nodes). (**b**) Degree at a carrier frequency of 16 Hz resolved in cortical space (LPC). The color scale is adjusted to the maximal and minimal degree that occurred. (**c**) Spectrally resolved number of nodes with significantly increased betweenness compared with the average betweenness value (voxel-wise permutation test for betweenness > average betweenness, corrected for the number of nodes, $P < 0.05$). (**d**) Betweenness at a carrier frequency of 16 Hz resolved in cortical space. Betweenness is statistically masked at two levels (permutation test, corrected for the number of nodes, $P < 0.05$, saturated color scale; permutation test, $P < 0.05$, uncorrected, desaturated color scale). The color scale is adjusted to the maximal and minimal betweenness in the statistical mask. (**e**) Spectrally resolved number of normalized betweenness nodes defined analogously to **c**. (**f**) Normalized betweenness at a carrier frequency of 16 Hz resolved in cortical space analogously to **d**.

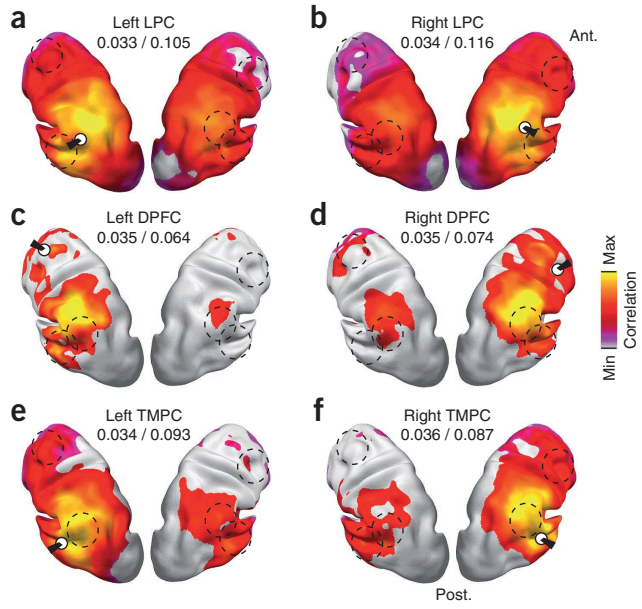

Figure 5 Correlation maps for identified hubs at a carrier frequency of 16 Hz. Correlation maps are statistically masked (voxel-wise one-sided *t* test for correlation > average correlation to the rest of the brain, $P < 0.05$, FDR corrected for the number of voxels). The white circles indicate the approximate location of the hub that was used as reference for the correlation analysis. The dashed lines indicate the locations of the other hubs. The values underneath the seed labels indicate the minimal and maximal correlation in the statistical mask. (**a**,**b**) Left and right LPC. (**c**,**d**) Left and right DPFC. (**e**,**f**) Left and right TMPC.

a connection if the correlation between the orthogonalized signals of two sources was significantly higher than the average correlation of these sources to the rest of the brain (one-sided *t* test, $P < 0.01$). We used graph-theoretical measures to quantify basic properties of the connectivity matrix[30]. The number of connections (termed degree) was highest for the alpha and beta carrier-frequency range (8–32 Hz), where it reached ~25% of all possible connections (**Fig. 4a**). The spatial distribution of the degree for this carrier-frequency range was characterized by a global anterior-to-posterior increase (**Fig. 4b**). Besides this strong gradient, the degree distribution peaked prominently in bilateral LPC with connections to ~85% of all sources (MNI coordinates: left, [−39, −54, 32]; right, [46, −45, 39]).

The prominent role of LPC was further supported by its high level of betweenness. Betweenness quantifies the number of all possible shortest paths in a network a given node participates in. It therefore complements degree as a measure that quantifies a node's importance for mediating connectivity between other nodes, that is, it's 'hubness'. For carrier frequencies in the alpha to beta frequency range (8–32 Hz), the number of significant betweenness nodes (permutation test, $P < 0.05$, corrected) and the spatial betweenness distribution qualitatively resembled the degree (**Fig. 4c**,**d**), with prominent maxima in bilateral LPC.

High degree favors high betweenness. Nodes with many connections are more likely to support the shortest paths between many other nodes. To account for this bias, we computed normalized betweenness, that is, the betweenness corrected for betweenness that occurs in random networks with the same degree. The number of voxels with significant normalized betweenness peaked sharply at 16 Hz (permutation test, $P < 0.05$, corrected; **Fig. 4e**). In addition to LPC, this procedure exposed hubs in medial and bilateral dorsal prefrontal cortex (MNI coordinates: MPFC, [10, 60, 10]; left DPFC, [−40, 30, 50]; right DPFC, [30, 20, 30]) and bilateral temporal cortex (TMPC; MNI coordinates: left, [−50, −40, −10]; right, [60, −20, 0]; **Fig. 4f**).

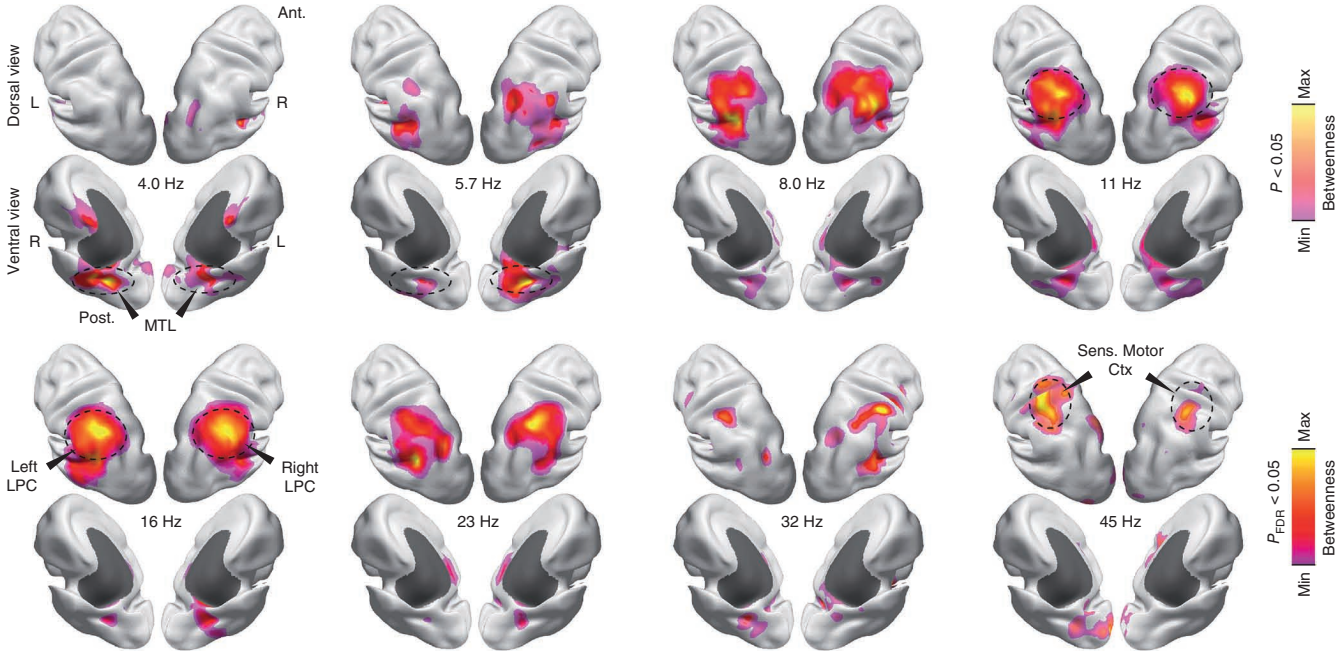

Figure 6 Spatial patterning of betweenness as a function of the carrier frequency. Betweenness values are statistically masked (voxel-wise permutation test for betweenness > average betweenness, corrected for number of nodes, $P < 0.05$, saturated color scale; $P < 0.05$, uncorrected, desaturated color scale). The color scale is adjusted to the minimal and maximal values in the statistical mask. Subcortical areas are masked dark gray (see **Supplementary Fig. 4** for complementary analysis of degree). Sens., sensory; Ctx, cortex.

The pattern of connectivity at 16 Hz differed between the LPC, MPFC, DPFC and TMPC. The high degree of bilateral LPC was driven by a widespread correlation with large parts of the brain (*t* test for correlation > average correlation, $P < 0.05$, FDR corrected; **Fig. 5a**,**b**). The correlation was strongest to the vicinity of the LPC and to the LPC in the other hemisphere. In contrast, the hubs in bilateral MPFC, DPFC and TMPC were characterized by sparser connectivity (**Figs. 3d** and **5c**–**f**). Notably, most of the hub sites showed mutual peaks in the spatial correlation patterns. Thus, the LPC, MPFC, DPFC and TMPC were not diffusely connected, but formed an interconnected network.

Global correlation structure varies with carrier frequency

The above analyses focused on a carrier frequency of 16 Hz. To investigate whether the global correlation structure varies across carrier frequencies, we performed a two-way analysis of variance of the carrier frequency–dependent connectivity (4–45 Hz) with the factors carrier frequency and cortical location. Indeed, degree and betweenness showed significant main and interaction effects (degree: main effect carrier frequency, $F_7 = 4.88 \times 10^4$, $P = 0$; main effect location, $F_{2924} = 102$, $P = 0$; interaction, $F_{7,2924} = 9.88$, $P = 0$; betweenness: main effect carrier frequency, $F_7 = 203$, $P = 5.15 \times 10^{-302}$; main effect location, $F_{2924} = 8.29$, $P = 0$; interaction, $F_{7,2924} = 1.12$, $P = 8.01 \times 10^{-31}$). Thus, degree and betweenness were not only spatially inhomogeneous, but the spatial patterning of connectivity also depended on the underlying carrier frequency.

The frequency-dependent degree revealed three prominent patterns of connectivity (**Fig. 6**). In the theta range (4–6 Hz), we found the highest degree in the medial temporal lobe (MTL, MNI coordinates, left, [−20, −40, −10]; right, [40, −40, 0]). Consistent with the above results, for frequencies in the alpha to beta frequency range (8–23 Hz), LPC showed the highest degree. In the low gamma frequency range (32–45 Hz), we found the highest degree in sensorimotor cortex (MNI coordinates, left, [−40, −40, 60]; right, [40, −30, 50]). These results were consistent with the patterns that we found for the frequency-dependent betweenness (**Supplementary Fig. 4**). In summary, the graph-theoretical analysis of global connectivity revealed spatially symmetric connectivity structure and localized hubs that depended on the underlying carrier frequency.

DISCUSSION

Here we introduce a new analysis approach for characterizing brain-wide functional connectivity based on power envelope correlation that overcomes limitations resulting from the limited spatial resolution of electrophysiological measures. Applying this approach to MEG, we provide a spectrally resolved characterization of the global organization of spontaneous electrophysiological signals in the human brain. The correlation of band-limited neuronal population activity showed prominent hubs that were largely symmetric across hemispheres and depended on the underlying carrier frequency.

Power envelope correlations between orthogonalized signals

Central for our findings was the new analysis approach for estimating power envelope correlations on the basis of orthogonalized signals. We applied this approach to MEG source estimates of spontaneous activity fluctuations of the resting human brain. However, because the underlying physical principles hold for both magnetic and electric fields, this approach should be similarly powerful for the analysis of EEG data. Furthermore, our approach is not limited to the analysis of spontaneous activity, but may also provide new insights into task-related functional connectivity. In general, the approach can be applied to any set of simultaneous electrophysiological signals to derive an index for functional connectivity, which may be relevant for biomedical applications.

The combination of EEG or MEG with our analysis approach complements electrocorticogram (ECoG) recordings, which have a higher spatial resolution and signal-to-noise ratio, but are limited to a few focal sites and studies of the diseased brain[27,31,32]. In fact, our analysis approach may also help in the investigation of correlations between signals from nearby ECoG or microelectrode recordings that may also be affected by spurious correlations resulting from limited spatial resolution.

The applied analysis approach can provide a full connectivity matrix, which allows for studying brain-wide correlation using graph-theoretical methods. It is straightforward to apply this analysis approach to contrasting groups of subjects or experimental conditions. The orthogonalization approach may also be combined with multivariate methods such as independent component analysis (ICA) to identify networks of areas with correlated power envelopes[29]. Furthermore, nonlinear or directed measures of interaction may also be applied to the power envelopes of orthogonalized signals.

The global correlation depends on the carrier frequency

We found that the global correlation of spontaneous activity peaked for carrier frequencies in the alpha to beta range with prominent hubs in the LPC and secondary hubs in PFC and TMPC. These hubs resemble the hub structures reported for spontaneous hemodynamic signals[8]. We found that all of these hubs were not diffusely connected, but were strongly correlated with each other as a global network. This network structure is compatible with the spatial pattern extracted from spontaneous MEG power fluctuations in the alpha to beta band using ICA[29]. The identified network overlaps with two networks in the correlation of hemodynamic signals: the default mode network[2,3,33], which comprises areas typically deactivated during tasks, and the control network[5,7], which has been implicated in executive functions. Besides this global structure, for the same alpha to beta carrier-frequency range, our analysis revealed spatially distinct correlations between functionally related sensory and associative cortices. These results substantiate converging evidence from MEG[28,29,34–36] and EEG[37–39] of the resting brain that suggest a prominent correlation of oscillatory power in particular in the alpha to beta frequency range. Thus, correlation of alpha to beta activity may be a generic signature of intrinsic neuronal interactions.

In addition to the prominent effects in the alpha to beta band, we found spatially specific correlation structure of spontaneous activity for a wide range of carrier frequencies from the theta to the gamma band (4–45 Hz). In the theta frequency range (4–6 Hz), the MTL constituted a global hub. Theta-band oscillations are a prominent feature of neuronal dynamics in the MTL. They seem to be tightly related to memory processes and are phase-coupled to neuronal activity in other cortical regions[40–42]. In addition, studies of fMRI connectivity have identified mnemonic networks that involve the MTL[4,6]. Consistent with these findings, our results suggest that the MTL is central to the brain-wide co-variation of spontaneous theta-band activity.

Timescale of power envelope correlations

Consistent with other MEG[28,35,36] and intracranial recordings[27,43], we found that correlations of oscillatory power were driven by slow co-variations in a broad frequency range below 0.1 Hz. Similarly, hemodynamic correlations are dominated by frequencies below 0.1 Hz[26]. These slow co-fluctuations may arise from intrinsic cortical dynamics[44] and subcortical or neuromodulatory inputs[18,19,43,45]. The slow timescale of power envelope correlations contrasts with the

millisecond timescale of neuronal signaling itself. Power envelope correlations likely reflect the consequence of signaling rather than acting as a mechanism that controls the signaling on a fast timescale.

Relation to local neuronal activity

In the raw EEG or MEG of awake humans, alpha and beta oscillations are the most prominent rhythms. One could speculate that the strong correlations in the alpha and beta frequency range simply reflect the better signal-to-noise ratio of these prominent local signals. However, differences in the spatial characteristics argue against this explanation. Local alpha and beta oscillations appear to be widespread across occipital, parietal and central areas (**Supplementary Fig. 5**). This pattern differs substantially from the global hub structure that we identified in this frequency range based on power envelope correlations (**Fig. 6**). In addition, for other frequencies, the hub structure differs substantially from the spatial distribution of local signal power. Thus, the strength of local oscillatory processes and their brain-wide spatial correlation are dissociated. Consequently, the correlation of signal power may provide complementary information to local signal power that could be exploited in future applications.

Relation to fMRI

EEG and MEG allow for separating neuronal activity into oscillatory components that reflect the biophysical properties of different local and large-scale network processes[17–19]. In contrast, fMRI provides a compound measure of the joint metabolic cost of different network processes and of non-neuronal processes[14–16,18]. This compound nature of the hemodynamic signal is reflected in its correlation with oscillatory neuronal activity across a broad range of frequencies during stimulation[46–48] and at rest[37–39,45,49]. Thus, the correlation structure of electrophysiological and hemodynamic signals should share similarities. Indeed, the patterning and the timescale of electrophysiological signal correlation that we found showed substantial similarities with fMRI connectivity (see above).

However, despite these similarities, the spatial structure of power envelope correlations also exhibited differences to hemodynamic correlation. In particular, hemodynamic correlation is characterized by prominent hubs in the posterior midline[2,8,33], which were largely absent in the electrophysiological connectivity that we observed and in networks extracted from MEG using ICA[29]. This apparent discrepancy may reflect the different nature of electrophysiological and hemodynamic signals. Furthermore, it should be taken into account that source estimates from EEG and MEG may have a spatially inhomogeneous sensitivity, which might result in an attenuation of deep sources.

Power envelope correlation in the gamma frequency range

Neuronal oscillations in the gamma frequency range have been found in various experimental contrasts and may be a generic signature of local cortical activity[18,22]. A growing number of combined electrophysiology and fMRI studies have linked hemodynamic signals to neuronal activity, particularly in the gamma band[45,46,48–50]. These findings suggest that resting state functional connectivity observed using fMRI[2] may manifest in the correlation of oscillatory activity in the gamma frequency range. This notion is supported by invasive ECoG studies that found long-range power correlation in this frequency range[27,31].

In contrast, we did not find prominent global correlation in the gamma frequency range. This seemingly unexpected finding may relate to different issues. First, the source of variance that drives the neuronal signals likely has a profound influence[18]. Sensory stimulation effectively drives cortical gamma-band activity[18,46] that can be measured with EEG and MEG[21,23,48]. In contrast, during rest, gamma-band fluctuations may be much smaller and the global correlation may be dominated by alpha to beta band activity. Second, the spatial sampling of recorded signals is likely to be important. Compared with intracranial electrodes, EEG and MEG average over larger populations of neurons. As a consequence, EEG and MEG may be particularly sensitive to spectral components with a broader spatial coherence, whereas intracranial measures may be more sensitive to locally coherent rhythms. Non-invasive and invasive measures may therefore emphasize signals with different spatial and spectral characteristics.

METHODS

Methods and any associated references are available in the online version of the paper.

Note: Supplementary information is available in the online version of the paper.

ACKNOWLEDGMENTS

We thank C. Hipp for helpful discussions and comments on the manuscript, and the bwGRiD project (http://www.bw-grid.de) for the computational resources. This work was supported by grants from the European Union (NEST-PATH-043457 to A.K.E. and HEALTH-F2-2008-200728 to M.C. and A.K.E.) and the National Institute of Mental Health (R01 MH096482-01 to M.C.).

AUTHOR CONTRIBUTIONS

All of the authors designed the experiment and wrote the paper. J.F.H. and D.J.H. collected the data and performed the data analysis. J.F.H. conceived the orthogonalization approach.

COMPETING FINANCIAL INTERESTS

The authors declare competing financial interests: details accompany the online version of the paper.

Published online at http://www.nature.com/doifinder/10.1038/nn.3101.
Reprints and permissions information is available online at http://www.nature.com/reprints/index.html.

1. Biswal, B., Yetkin, F.Z., Haughton, V.M. & Hyde, J.S. Functional connectivity in the motor cortex of resting human brain using echo-planar MRI. *Magn. Reson. Med.* **34**, 537–541 (1995).
2. Fox, M.D. & Raichle, M.E. Spontaneous fluctuations in brain activity observed with functional magnetic resonance imaging. *Nat. Rev. Neurosci.* **8**, 700–711 (2007).
3. Fox, M.D. *et al.* The human brain is intrinsically organized into dynamic, anticorrelated functional networks. *Proc. Natl. Acad. Sci. USA* **102**, 9673–9678 (2005).
4. Vincent, J.L. *et al.* Coherent spontaneous activity identifies a hippocampal-parietal memory network. *J. Neurophysiol.* **96**, 3517–3531 (2006).
5. Vincent, J.L., Kahn, I., Snyder, A.Z., Raichle, M.E. & Buckner, R.L. Evidence for a frontoparietal control system revealed by intrinsic functional connectivity. *J. Neurophysiol.* **100**, 3328–3342 (2008).
6. Kahn, I., Andrews-Hanna, J.R., Vincent, J.L., Snyder, A.Z. & Buckner, R.L. Distinct cortical anatomy linked to subregions of the medial temporal lobe revealed by intrinsic functional connectivity. *J. Neurophysiol.* **100**, 129–139 (2008).
7. Dosenbach, N.U.F. *et al.* Distinct brain networks for adaptive and stable task control in humans. *Proc. Natl. Acad. Sci. USA* **104**, 11073–11078 (2007).
8. Buckner, R.L. *et al.* Cortical hubs revealed by intrinsic functional connectivity: mapping, assessment of stability, and relation to Alzheimer's disease. *J. Neurosci.* **29**, 1860–1873 (2009).
9. Power, J.D. *et al.* Functional network organization of the human brain. *Neuron* **72**, 665–678 (2011).
10. Lewis, C.M., Baldassarre, A., Committeri, G., Romani, G.L. & Corbetta, M. From the cover: learning sculpts the spontaneous activity of the resting human brain. *Proc. Natl. Acad. Sci. USA* **106**, 17558–17563 (2009).
11. Dehaene, S. & Changeux, J.-P. Experimental and theoretical approaches to conscious processing. *Neuron* **70**, 200–227 (2011).
12. Zhang, D. & Raichle, M.E. Disease and the brain's dark energy. *Nat Rev Neurol.* **6**, 15–28 (2010).
13. Hawellek, D.J., Hipp, J.F., Lewis, C.M., Corbetta, M. & Engel, A.K. Increased functional connectivity indicates the severity of cognitive impairment in multiple sclerosis. *Proc. Natl. Acad. Sci. USA* **108**, 19066–19071 (2011).
14. Logothetis, N.K. What we can do and what we cannot do with fMRI. *Nature* **453**, 869–878 (2008).

15. Sirotin, Y.B. & Das, A. Anticipatory haemodynamic signals in sensory cortex not predicted by local neuronal activity. *Nature* **457**, 475–479 (2009).
16. Heeger, D.J. & Ress, D. What does fMRI tell us about neuronal activity? *Nat. Rev. Neurosci.* **3**, 142–151 (2002).
17. Wang, X.-J. Neurophysiological and computational principles of cortical rhythms in cognition. *Physiol. Rev.* **90**, 1195–1268 (2010).
18. Donner, T.H. & Siegel, M. A framework for local cortical oscillation patterns. *Trends Cogn. Sci.* **15**, 191–199 (2011).
19. Siegel, M., Donner, T.H. & Engel, A.K. Spectral fingerprints of large-scale neuronal interactions. *Nat. Rev. Neurosci.* **13**, 121–134 (2012).
20. Bruns, A., Eckhorn, R., Jokeit, H. & Ebner, A. Amplitude envelope correlation detects coupling among incoherent brain signals. *Neuroreport* **11**, 1509–1514 (2000).
21. Siegel, M., Donner, T.H., Oostenveld, R., Fries, P. & Engel, A.K. Neuronal synchronization along the dorsal visual pathway reflects the focus of spatial attention. *Neuron* **60**, 709–719 (2008).
22. Fries, P. Neuronal gamma-band synchronization as a fundamental process in cortical computation. *Annu. Rev. Neurosci.* **32**, 209–224 (2009).
23. Hipp, J.F., Engel, A.K. & Siegel, M. Oscillatory synchronization in large-scale cortical networks predicts perception. *Neuron* **69**, 387–396 (2011).
24. Nolte, G. *et al.* Identifying true brain interaction from EEG data using the imaginary part of coherency. *Clin. Neurophysiol.* **115**, 2292–2307 (2004).
25. Schoffelen, J.-M. & Gross, J. Source connectivity analysis with MEG and EEG. *Hum. Brain Mapp.* **30**, 1857–1865 (2009).
26. Cordes, D. *et al.* Frequencies contributing to functional connectivity in the cerebral cortex in 'resting-state' data. *AJNR Am. J. Neuroradiol.* **22**, 1326–1333 (2001).
27. Nir, Y. *et al.* Interhemispheric correlations of slow spontaneous neuronal fluctuations revealed in human sensory cortex. *Nat. Neurosci.* **11**, 1100–1108 (2008).
28. Brookes, M.J. *et al.* Measuring functional connectivity using MEG: methodology and comparison with fcMRI. *Neuroimage* **56**, 1082–1104 (2011).
29. Brookes, M.J. *et al.* Investigating the electrophysiological basis of resting state networks using magnetoencephalography. *Proc. Natl. Acad. Sci. USA* **108**, 16783–16788 (2011).
30. Rubinov, M. & Sporns, O. Complex network measures of brain connectivity: uses and interpretations. *Neuroimage* **52**, 1059–1069 (2010).
31. He, B.J., Snyder, A.Z., Zempel, J.M., Smyth, M.D. & Raichle, M.E. Electrophysiological correlates of the brain's intrinsic large-scale functional architecture. *Proc. Natl. Acad. Sci. USA* **105**, 16039–16044 (2008).
32. Miller, K.J., Weaver, K.E. & Ojemann, J.G. Direct electrophysiological measurement of human default network areas. *Proc. Natl. Acad. Sci. USA* **106**, 12174–12177 (2009).
33. Greicius, M.D., Krasnow, B., Reiss, A.L. & Menon, V. Functional connectivity in the resting brain: a network analysis of the default mode hypothesis. *Proc. Natl. Acad. Sci. USA* **100**, 253–258 (2003).
34. Bassett, D.S., Meyer-Lindenberg, A., Achard, S., Duke, T. & Bullmore, E. Adaptive reconfiguration of fractal small-world human brain functional networks. *Proc. Natl. Acad. Sci. USA* **103**, 19518–19523 (2006).
35. Liu, Z., Fukunaga, M., de Zwart, J.A. & Duyn, J.H. Large-scale spontaneous fluctuations and correlations in brain electrical activity observed with magnetoencephalography. *Neuroimage* **51**, 102–111 (2010).
36. de Pasquale, F. *et al.* Temporal dynamics of spontaneous MEG activity in brain networks. *Proc. Natl. Acad. Sci. USA* **107**, 6040–6045 (2010).
37. Laufs, H. *et al.* Electroencephalographic signatures of attentional and cognitive default modes in spontaneous brain activity fluctuations at rest. *Proc. Natl. Acad. Sci. USA* **100**, 11053–11058 (2003).
38. Mantini, D., Perrucci, M.G., Del Gratta, C., Romani, G.L. & Corbetta, M. Electrophysiological signatures of resting state networks in the human brain. *Proc. Natl. Acad. Sci. USA* **104**, 13170–13175 (2007).
39. Jann, K., Kottlow, M., Dierks, T., Boesch, C. & Koenig, T. Topographic electrophysiological signatures of FMRI resting state networks. *PLoS ONE* **5**, e12945 (2010).
40. Buzsáki, G. Theta oscillations in the hippocampus. *Neuron* **33**, 325–340 (2002).
41. Fell, J. & Axmacher, N. The role of phase synchronization in memory processes. *Nat. Rev. Neurosci.* **12**, 105–118 (2011).
42. Battaglia, F.P., Benchenane, K., Sirota, A., Pennartz, C.M.A. & Wiener, S.I. The hippocampus: hub of brain network communication for memory. *Trends Cogn. Sci.* **15**, 310–318 (2011).
43. Leopold, D.A., Murayama, Y. & Logothetis, N.K. Very slow activity fluctuations in monkey visual cortex: implications for functional brain imaging. *Cereb. Cortex* **13**, 422–433 (2003).
44. Deco, G., Jirsa, V.K. & McIntosh, A.R. Emerging concepts for the dynamical organization of resting-state activity in the brain. *Nat. Rev. Neurosci.* **12**, 43–56 (2011).
45. Schölvinck, M.L., Maier, A., Ye, F.Q., Duyn, J.H. & Leopold, D.A. Neural basis of global resting-state fMRI activity. *Proc. Natl. Acad. Sci. USA* **107**, 10238–10243 (2010).
46. Logothetis, N.K., Pauls, J., Augath, M., Trinath, T. & Oeltermann, A. Neurophysiological investigation of the basis of the fMRI signal. *Nature* **412**, 150–157 (2001).
47. Goense, J.B.M. & Logothetis, N.K. Neurophysiology of the BOLD fMRI signal in awake monkeys. *Curr. Biol.* **18**, 631–640 (2008).
48. Scheeringa, R. *et al.* Neuronal dynamics underlying high- and low-frequency EEG oscillations contribute independently to the human BOLD signal. *Neuron* **69**, 572–583 (2011).
49. Magri, C., Schridde, U., Murayama, Y., Panzeri, S. & Logothetis, N.K. The amplitude and timing of the BOLD signal reflects the relationship between local field potential power at different frequencies. *J. Neurosci.* **32**, 1395–1407 (2012).
50. Mukamel, R. *et al.* Coupling between neuronal firing, field potentials, and FMRI in human auditory cortex. *Science* **309**, 951–954 (2005).

ONLINE METHODS

MEG recording. MEG was continuously recorded with a 275-channel whole-head system (Omega 2000, CTF Systems) in a magnetically shielded room. The electro-oculogram was recorded simultaneously for off-line artifact rejection. The head position relative to the MEG sensors was measured continuously using a set of head localization coils (nasion, left and right ears). MEG signals were low-pass filtered online (cutoff = 300 Hz) and recorded with a sampling rate of 1,200 Hz.

Subjects and experimental procedure. Subjects (n = 43, age = 25.5 ± 3.5 years, mean ± s.d., 21 females) fixated a cross projected centrally onto a back projection screen with an LCD projector (Sanyo Pro Xtrax PLC-XP51) from outside the magnetically shielded room. Subjects were instructed to continuously maintain fixation (duration = 505 ± 115 s, mean ± s.d., range = 360–620 s). The study was conducted in accordance with the Declaration of Helsinki and informed consent was obtained from all participants before the recordings.

Preprocessing and artifact rejection. The data were high-pass filtered offline (cut-off = 0.5 Hz, Butterworth, fourth order) and artifactual data (eye movements, strong muscle activity) were rejected on the basis of visual inspection (13.4 ± 7.6%, mean ± s.d.; range = 2.1–39.5%). For the analysis of spectral components above 32 Hz, we performed additional cleaning to account for muscular artifacts. The data were high-pass filtered (30 Hz, Butterworth, fourth order), ICA was computed and artifactual components related to muscular activity were rejected from the data (7 ± 3.8, mean ± s.d.; range = 1–16).

Analysis software. All data analyses were performed in Matlab (MathWorks) using custom scripts and open source toolboxes: Fieldtrip[51] (http://www.ru.nl/fcdonders/fieldtrip/), SPM2 (http://www.fil.ion.ucl.ac.uk/spm/), Brain Connectivity Toolbox[30] (http://www.brain-connectivity-toolbox.net/).

Spectral analysis. We derived spectral estimates using Morlet's wavelets[52] $w(t,f)$

$$w(t,f) = (\sigma_t\sqrt{\pi})^{-1/2} e^{-t^2/2\sigma_t^2} e^{-i2\pi ft}$$

Here, f is the center frequency (carrier frequency) and σ_t is the temporal s.d. The time-frequency estimate $X(t,f)$ of a signal $x(t)$ was then computed by convolution with $w(t,f)$

$$X(t,f) = x(t) * w(t,f)$$

We chose a spectral band-width of 1/2 octave (corresponding to f/σ_f ~5.83; σ_f, spectral s.d.) and spaced the center frequencies logarithmically according to the exponentiation of the base 2 with exponents ranging from 1 to 7 in steps of 1/4. We derived spectral estimates in successive half-overlapping temporal windows that covered $\pm 3\sigma_t$. For time points at which the convolution kernel overlapped with sections marked as artifacts (see preprocessing), the data were discarded.

Source locations and physical forward model. For source analyses, we used three different source configurations defined in MNI space. For correlation maps of selected reference locations, spatial normalization of correlation values for statistical testing (see below) and the all-to-all analysis, we used a regular three-dimensional grid that covered the whole brain (1-cm spacing, 2,925 source locations; for co-variation frequency analyses we used 2-cm spacing, 369 source locations). For the correlation analysis between homologous sensory areas, we defined bilateral sensory locations in MNI space. The coordinates of the sensory regions were identified by a meta-analysis of fMRI literature using the BrainMap.org resources[53] (auditory cortex ([−54, −22, 10], [52, −24, 12]), somatosensory cortex ([−42, −26, 54], [38, −32, 48]), visual cortex ([−20, −86, 18], [16, −80, 26]). Locations of interest derived from fMRI correlation literature[3] for seed correlation analyses: l/r MT+ ([−47, −69, −3], [54, −63, −8]), MPFC ([−3, 39, −2]) and SMA ([−2, 1, 51]).

For source analysis, we constructed individual physical forward models (leadfields). We affine-transformed source locations into individual head space using the participants' individual T1-weighted structural MRI and aligned the MEG sensors to the head geometry on the basis of three fiducial points (nasion, and left and right ear, registered during the MEG acquisition by three head localization coils). To derive the physical relation between sources and sensors, we employed a single-shell model[54].

Source analysis. We used adaptive linear spatial filtering (beamforming)[23,55,56] to estimate the spectral amplitude and phase of neuronal signals at the source level. For each frequency f and source location r, three orthogonal filters ($\hat{A} = [A_1, A_2, A_3]$; one for each spatial dimension) were computed that pass activity from location r with unit gain while maximally suppressing activity from all other sources

$$\hat{A}(r,f) = \left[L^T(r)C_{\text{real}}(f)^{-1}L(r)\right]^{-1} L^T(r)C_{\text{real}}(f)^{-1}$$

Here, $L(r)$ is a matrix whose columns are the leadfields of three orthogonal dipoles at source location r, C_{real} denotes the real part of the complex cross-spectral-density matrix for the sensor level data at frequency f and T indicates the matrix transpose. We linearly combined the three filters to a single filter pointing in the direction of maximal variance, that is, the dominant dipole orientation. To this end, the filters were weighted with the first eigenvectors' elements (the eigenvector with the largest eigenvalue of the real part of the cross-spectral-density matrix at the source location r)

$$v(r,f) = [v_1(r,f), v_2(r,f), v_3(r,f)] = Eig_1\left(\hat{A}(r,f)C_{\text{real}}(f)\hat{A}(r,f)^{*T}\right)$$

$$A(r,f) = v_1(r,f)A_1(r,f) + v_2(r,f)A_2(r,f) + v_3(r,f)A_3(r,f)$$

To derive the complex source estimates, the complex frequency domain data were then multiplied with the real-valued filter

$$X_{\text{source}}(r,t,f) = A(r,f)X_{\text{sensor}}(t,f)$$

Here, $X_{\text{sensor}}(t,f)$ is the frequency domain representation of the sensor level data at time t and frequency f, and $X_{\text{source}}(r,t,f)$ is the corresponding source signal at location r. To account for the spatial bias of the beamforming solution when investigating signal power (**Supplementary Fig. 5**), we jointly normalized the three leadfields for each source location by division with the sum of all squared values.

Power envelope correlation between orthogonalized signals. Here we provide a brief account of the applied method. Please see **Supplementary Data** and **Supplementary Figures 1** and **2** for additional information and numerical simulations on this approach.

We assessed neuronal interactions by quantifying correlations between power envelopes[19,20,57,58]. To this end, we squared the absolute values of the complex spectral estimates and applied a logarithmic transform to render the power statistics more normal. We then computed Pearson's linear correlation between the resulting power envelopes from two different locations.

To discount spurious correlations caused by the limited spatial resolution of source estimates, we orthogonalized any two time series of band-limited activity before computing their power envelopes. We performed this operation in the frequency domain. We defined the complex signal $Y(t,f)$ orthogonalized to the complex signal $X(t,f)$ (see **Supplementary Fig. 1**)

$$Y_{\perp X}(t,f) = \text{imag}\left(Y(t,f)\frac{X(t,f)^*}{|X(t,f)|}\right)$$

The orthogonalization can be done in two directions (X to Y, Y to X). We computed power envelope correlations for both directions of orthogonalized time-series and averaged the values for subsequent analysis. We performed the orthogonalization time point by time point, which requires no assumption about stationarity of the signals' relation beyond the length of the carrier-frequency dependent analysis window. Discounting the non-orthogonal signal components leads to an underestimation of true correlation by a factor of ~0.577. This factor was accounted for when reporting correlation values between orthogonalized signals.

Spectrally resolved correlation of power envelopes (second level analysis). To resolve the correlation between two orthogonalized signals in frequency

(co-variation frequency), we applied spectral analysis to the power envelopes with an approach equivalent to using Morlet's wavelets. We chose a spectral bandwidth of 0.95 octaves ($f/\sigma_f \sim 3.15$) and spaced the center frequencies logarithmically according to the exponentiation of the base 10 with exponents ranging from −1.5 in steps of 0.1 to 1/6 of the carrier frequency. We derived spectral estimates in successive half-overlapping temporal windows that covered $\pm 3\sigma_t$. From these complex numbers, we derived the coherency between power envelopes and took the real part of coherency as the frequency-specific measure of correlation.

Power envelopes were interrupted by periods of missing data resulting from artifacts such as eye blinks or strong muscle activity. Thus, the convolution with Morlet's wavelets as described above was not feasible and we employed a spectral estimate approach that could cope with missing data. For discrete signals, time domain and frequency domain representations are linearly related

$$x = BX, \quad X = \mathrm{inv}(B)x$$

Here, x is the time domain representation, X is the frequency domain representation and B is the Fourier basis (that is, family of orthogonal complex sinusoids). For data with invalid temporal sections, B is rank deficient. In this case, we derived the spectral estimate employing the pseudo inverse.

$$X = \mathrm{pinv}(B)x$$

As a windowing function, we used a Gaussian taper such that if no data was missing, the approach was identical to using Morlet's wavelets. Data sections with more than 50% missing data were discarded from the analysis.

Statistical analysis of correlation structure and definition of connections. Across a broad range of frequencies, power envelope correlations between orthogonalized signals had a positive offset, that is, the brain-wide correlation was consistently larger than zero. To focus on the spatial correlation structure, we used Student's t-tests and identified correlation higher than the average correlation to all locations on a three-dimensional grid covering the brain. We corrected for multiple comparisons by controlling the FDR. Please note that this statistic depends on the sources across which the average correlation is estimated.

For the analysis of the global correlation structure, no particular reference location exists. For this case, the correlation between any two sites can statistically be compared to the brain-wide correlation of either one of the two sites. We established a symmetric connectivity measure by defining a connection to be present if statistics for either one of the two possible normalizations reached significance (we accounted for two tests by Bonferroni correction, $P_{\mathrm{threshold}} = 0.01/2$). This resulted in a symmetric connection matrix that was used for subsequent graph-theoretical analyses. The symmetrization allowed for fully connected nodes; in other words, there could be more than 50% connections (for example, see **Fig. 4b**).

Graph-theoretical analysis. We used graph-theoretical measures[30] to quantify basic properties of global connectivity. We employed three measures highlighting different aspects of the global correlation

Degree is represented as

$$D_i = \frac{1}{N-1}\sum_j a_{ij}$$

Here, D_i is the degree at location i, and a_{ij} is the connection (0 for no connection, 1 for a connection) between locations i and j, and N is the total number of connections. The total degree is the average of the degree at all locations.

Betweenness is represented as

$$B_i = \frac{1}{(N-1)(N-2)} \sum_{\substack{h,j \\ h\neq j, h\neq i, j\neq i}} \frac{\rho_{hj}(i)}{\rho_{hj}}$$

Here, B_i is the betweenness at location i, ρ_{hj} is the number of shortest paths between h and j, and $\rho_{hj}(i)$ is the number of shortest paths between h and j that passes through i.

The normalized betweenness is represented as

$$BN_i = \frac{B_i - \mathrm{mean}(B_i^{\mathrm{rand}})}{\mathrm{sd}(B_i^{\mathrm{rand}})}$$

Here, BN_i is the normalized betweenness at location i derived from the betweenness B_i and the mean and s.d. of a set of betweenness values B_i^{rand} (20 resamples) from connection matrices with identical degree but randomized connectivity[59]. Thus, normalized betweenness accounts for the betweenness that occurs in a random network with identical degree.

Statistical analysis of graph-theoretical measures. We performed random effects statistics to assess the modulation of graph-theoretical measures. We first derived single subject estimates of graph-theoretical measures using a jackknifing procedure. For each subject i of N subjects, we derived a robust jackknife resample R_i by averaging graph-theoretical measures from connectivity matrices based on all, but this subject and one other subject at a time. From these jackknife resamples, we computed single subject estimates G_i

$$G_i = \sum_{j=1}^{N} R_j - (N-1)R_i$$

This corresponds to pseudo-values without bias correction. Based on these estimates, we performed the following random-effects statistics.

To assess the spatial patterning of graph-theoretical measures, we employed random permutation statistics. We generated an empirical null hypothesis distribution for no spatial patterns by randomly permuting source locations for each subject and then computing the average across subjects (10,000 resamples). We selected only the largest value across the entire space of each resample to account for multiple testing. To assess the modulation of graph-theoretical measures with the factors carrier frequency and spatial location and their interaction, we performed a two-way analysis of variance.

Illustration of results. To illustrate the spatial distribution of correlation and graph-theoretical measures, we projected the quantities onto the cortical surface from the population-average, landmark- and surface-based atlas[60], or alternatively as an overlay on brain slices of the SPM99/2 template brain. We used different statistical masks as explained in the corresponding figure legends.

51. Oostenveld, R., Fries, P., Maris, E. & Schoffelen, J.-M. FieldTrip: open source software for advanced analysis of MEG, EEG, and invasive electrophysiological data. *Comput. Intell. Neurosci.* **2011**, 156869 (2011).
52. Tallon-Baudry, C., Bertrand, O., Delpuech, C. & Pernier, J. Stimulus specificity of phase-locked and non-phase-locked 40 Hz visual responses in human. *J. Neurosci.* **16**, 4240–4249 (1996).
53. Laird, A.R. *et al.* ALE meta-analysis workflows via the brainmap database: progress towards a probabilistic functional brain atlas. *Front. Neuroinform.* **3**, 23 (2009).
54. Nolte, G. The magnetic lead field theorem in the quasi-static approximation and its use for magnetoencephalography forward calculation in realistic volume conductors. *Phys. Med. Biol.* **48**, 3637–3652 (2003).
55. Van Veen, B.D., van Drongelen, W., Yuchtman, M. & Suzuki, A. Localization of brain electrical activity via linearly constrained minimum variance spatial filtering. *IEEE Trans. Biomed. Eng.* **44**, 867–880 (1997).
56. Gross, J. *et al.* Dynamic imaging of coherent sources: studying neural interactions in the human brain. *Proc. Natl. Acad. Sci. USA* **98**, 694–699 (2001).
57. Schepers, I.M., Hipp, J.F., Schneider, T.R., Röder, B. & Engel, A.K. Functionally specific oscillatory activity correlates between visual and auditory cortex in the blind. *Brain* **135**, 922–934 (2012).
58. Donner, T.H., Siegel, M., Fries, P. & Engel, A.K. Buildup of choice-predictive activity in human motor cortex during perceptual decision making. *Curr. Biol.* **19**, 1581–1585 (2009).
59. Maslov, S. & Sneppen, K. Specificity and stability in topology of protein networks. *Science* **296**, 910–913 (2002).
60. Van Essen, D.C.A. Population-average, landmark- and surface-based (PALS) atlas of human cerebral cortex. *Neuroimage* **28**, 635–662 (2005).

doi:10.1038/nn.3101